Analyst

MINIREVIEW

View Article Online
View Journal | View Issue

Cite this: *Analyst*, 2016, **141**, 5474

Recent advances in the development and application of nanoelectrodes

Yunshan Fan, Chu Han and Bo Zhang*

Nanoelectrodes have key advantages compared to electrodes of conventional size and are the tool of choice for numerous applications in both fundamental electrochemistry research and bioelectrochemical analysis. This Minireview summarizes recent advances in the development, characterization, and use of nanoelectrodes in nanoscale electroanalytical chemistry. Methods of nanoelectrode preparation include laser-pulled glass-sealed metal nanoelectrodes, mass-produced nanoelectrodes, carbon nanotube based and carbon-filled nanopipettes, and tunneling nanoelectrodes. Several new topics of their recent application are covered, which include the use of nanoelectrodes for electrochemical imaging at ultrahigh spatial resolution, imaging with nanoelectrodes and nanopipettes, electrochemical analysis of single cells, single enzymes, and single nanoparticles, and the use of nanoelectrodes to understand single nanobubbles.

Received 7th June 2016,
Accepted 26th July 2016

DOI: 10.1039/c6an01285j

www.rsc.org/analyst

1. Introduction

Nanoelectrodes, which are electrochemical probes with at least one dimension below 100 nm,[1] have received enormous attention in basic electrochemistry and electroanalytical research. This is largely due to several distinct advantages of nanoelectrodes compared to electrodes of conventional dimensions. The small size of a nanoelectrode enables one to probe faradaic reactions in extremely tight spaces, such as inside a single vesicle, a biological cell, or a single droplet, which are otherwise difficult or even impossible to measure with conventional electrodes. The miniaturized electrode size (and electrode area) also leads to insignificant electrical double layer capacitance and a small *RC* time constant. For example, a 10 nm electrode may have a double layer capacitance of ~30 aF and an *RC* time constant of the order of 30 fs in a normal electrolyte solution, *e.g.*, 0.1 M KCl. With such a small electrode, one can expect to run ultrafast voltammetric measurements using scan rates in the megavolt per second range and probe electrochemical processes in the nanosecond time scale. Another attractive feature of a nanoelectrode is the minimized *iR* drop due to the small faradaic current, often of the order of picoamperes (pA). This allows one to perform electrochemistry in a solution with very high electrical resistance containing little or

Department of Chemistry, University of Washington, Seattle, Washington 98115, USA. E-mail: zhangb@uw.edu; Fax: +1 206 685 8665; Tel: +1 206 543 1767

Yunshan Fan

Yunshan Fan received her B.S. in Polymer Materials Science & Engineering from Beijing Institute of Technology (China) in 2013. She then joined Professor Bo Zhang's lab at the University of Washington and is currently a Ph.D. student studying the electrochemical properties of single nanoparticles and single molecules using nanoelectrodes and fluorescence-enabled electrochemical microscopy (FEEM).

Chu Han

Chu Han received her B.S. in Materials Science & Engineering from the University of Science and Technology of China in 2013. She then joined Professor Bo Zhang's lab at the University of Washington and is currently a Ph.D. student investigating electrochemical coupling at a bipolar electrode when the electrode approaches the limit of a single nanoparticle.

even no added supporting electrolyte. Additionally, tremendous advances have been seen in the use of the steady-state voltammetric response of nanoelectrodes to analyze fast electron-transfer kinetics.

In this review, we wish to summarize recent advances in the area of development, characterization, and use of nanoelectrodes in fundamental electrochemistry and electroanalytical chemistry. Although several excellent reviews are available on similar topics,[1–5] we focus our attention on the new advances that have not yet been greatly covered in the recent literature. Here, we will start with a discussion of some of the most exciting new methods in the preparation and characterization of nanoelectrodes. These include the use of a laser puller to prepare glass-sealed metal nanoelectrodes, mass-fabricated metal pyramid nanoelectrodes, nanoelectrodes based on the use of carbon nanotubes, carbon-filled nanopipettes, and tunneling nanoelectrodes based on the immobilization of a single nanoparticle (NP) on an insulated ultramicroelectrode (UME). In the second part of this review, since the application of nanoelectrodes is rather broad, we chose to focus on several new topics of the recent application of nanoelectrodes in fundamental electrochemistry and electroanalysis. Selected topics include the use of nanoelectrodes to achieve ultrahigh spatial resolutions in scanning electrochemical microscopy (SECM) and new ideas on the combined use of SECM and atomic force microscopy (AFM) or scanning ion-conductance microscopy (SICM), studies of single cells, single-enzyme electrochemistry, single-NP electrochemistry, and the use of nanoelectrodes to form and better understand individual nanobubbles.

2. New fabrication methods

2.1 Glass-sealed metal nanoelectrodes

Laser pulling continues to be one of the most popular methods for the quick preparation of metal disk nanoelectrodes. This method uses a laser puller to heat up, stretch, and break a piece of metal wire, usually Pt or Au, pre-sealed inside a glass or quartz capillary, to produce a pair of ultrasharp metal tips. These tips are pre-sealed in glass or quartz and can be subsequently etched or mechanically polished to expose the metal disk surface. This method allows one to make nanoelectrodes of Pt, Ag, and Au[6–11] and the electrode size can be varied by adjusting the parameters in the pulling and polishing. Nanoelectrodes of other metals, such as Hg, can also be made through metal deposition on a laser-pulled Pt electrode.[12,13] Laser-pulled nanoelectrodes are often very challenging to polish without tip breakage. A 10 nm diameter laser-pulled nanoelectrode has an overall size usually below 400 nm. To make polishing more reproducible, one can seal the ultrasharp quartz tip into a larger 2 mm glass capillary. This has led to the successful fabrication of Au disk nanoelectrodes with radii as small as 5 nm[14] and Pt disk nanoelectrodes down to 1 nm.[15] A very attractive method for tip exposure is the use of focused-ion beam (FIB) milling, in which glass and metal atoms are sputtered off the tip by high-energy ions under vacuum. FIB milling allows one to precisely control tip exposure with sub-50 nm spatial resolution. Mirkin and Amemiya have used FIB milling to prepare nanoelectrodes of carbon.[16]

Dual nanoelectrodes with radii smaller than 100 nm can be prepared with a *θ*-glass pipette. Sun and coworkers have reported integrated dual disk nanoelectrodes with electrode spacing of the order of 1–2 μm.[17] They first laser pulled a *θ*-glass pipette into an hourglass shape, and then inserted one piece of Pt wire into each barrel. The two Pt wires were then heated with a laser and pulled together to produce well-sealed dual nanoelectrodes. The resulting electrodes can be polished to have radii varying from several tens to several hundred nanometers. The two Pt electrodes in the *θ*-glass pipette may be used independently or in the generation–collection mode.

The laser pulling method allows one to fabricate nanoelectrodes down to a few nm with bench-top equipment. However, it is difficult to produce electrodes with consistent shapes and sizes. The quality and reproducibility of electrodes often strongly depend on the condition of the laser puller and the experience of the operator, and the resulting electrode size can be difficult to predict without careful characterization. However, this is still an attractive method for quick fabrication of metal nanoelectrodes which can be easily adopted by many laboratories.

2.2 Mass-produced metal pyramid nanoelectrodes

Conductive, ultra-sharp metal pyramids are attractive nanostructures that can be used as nanoelectrodes. First developed by the Oh group, Au pyramids with a nanometer-sized tip (10 nm) can be mass-fabricated in a clean room using a template-stripping technique.[18] Specifically, a 100 nm thick layer of insulating Si_3N_4 was grown on a silicon wafer and an array of uniform micron-sized holes were produced in the nitride film using photolithography. Using the Si_3N_4 layer as an etching mask, the silicon wafer was then anisotropically etched in a concentrated KOH solution to create pyramidal molds. Next, a layer of 200 nm Au was deposited into the molds and the nitride mask was removed. After this, a single

Bo Zhang

Bo Zhang is an Associate Professor at the University of Washington. He obtained his Ph.D. working with Henry White at the University of Utah in 2006 and did postdoctoral work with Andrew Ewing before joining the UW in 2008. His current research is focused on the use of nanoelectrochemical tools to better understand chemical reactions at the electrode/solution interface and neuronal communication in the brain. His group uses massive electrochemical arrays and FEEM to image fast dynamic redox events.

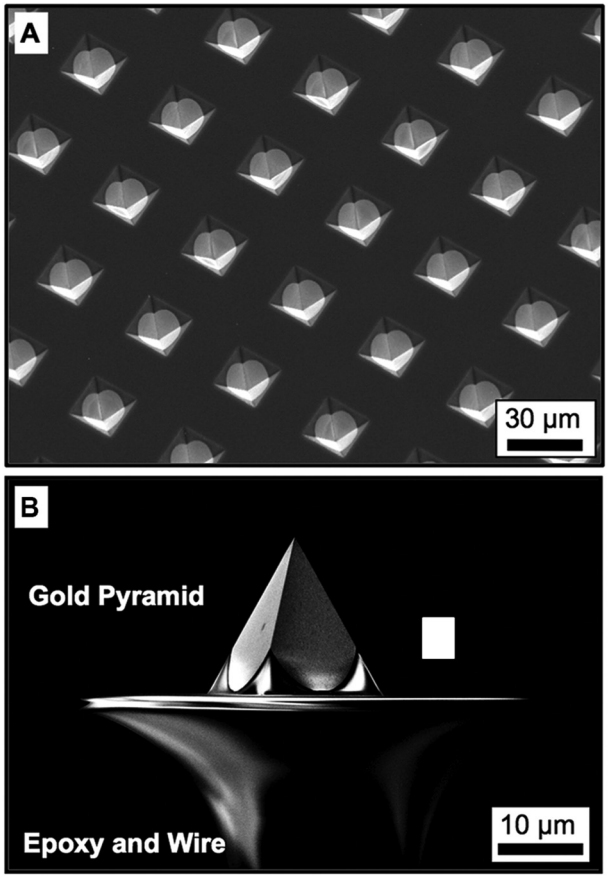

Fig. 1 Scanning electron microscopy (SEM) images of template-stripped Au pyramidal tips. (A) Massively produced uniform Au pyramids. (B) A single Au pyramidal tip plucked from the mold using epoxy and a short piece of tungsten wire. Adapted with permission from Johnson *et al.*[18] Copyright 2012 American Chemical Society.

Au pyramidal tip could be template stripped and lifted up using a tungsten wire with a small droplet of epoxy. This fabrication method has the advantage of high yield (>95%) and high reproducibility, resulting in massively produced (1.5 million nearly identical tips over a 4-inch wafer) uniform Au pyramids (Fig. 1).

In a recent report, Au pyramids were used as near-field imaging probes in fluorescence and Raman scattering with a spatial resolution down to 20 nm and a fluorescence enhancement factor of about 200.[18] If coupled with an indium tin oxide (ITO) electrode, the pyramid tip can also function as a three-dimensional dielectrophoretic trap to manipulate submicron particles.[19] With the ability to reproducibly and massively produce pyramids of different metals (*e.g.*, Au and Ag) with nanometer-sized tips of tunable taper angles,[20] this template-stripping technique demonstrates great potential in the fabrication of nanoelectrodes for electrochemical applications.

2.3. Carbon nanotube-based nanoelectrodes

Carbon nanotubes (CNTs) have attracted much attention due to their unique structural and electrical properties.[21,22] First demonstrated by Dekker and coworkers,[23,24] a single-walled carbon nanotube (SWCNT) can be used as a nanoelectrode for electrochemistry. To fabricate an electrochemical SWCNT device, they grew a SWCNT using chemical vapor deposition (CVD) on a substrate and established a contact by using titanium leads covered by a poly(methyl methacrylate) (PMMA) insulating layer. Using the SWCNT devices, they obtained steady-state electrochemical currents that scale with the exposed length of the SWCNT. They also observed similar steady-state voltammetric curves from metallic and semiconducting SWCNTs.

Nanoelectrodes based on a single CNT could also be fabricated by attaching a single multi-walled carbon nanotube (MWCNT) to a tungsten probe or a carbon fiber. Shen *et al.* fabricated CNT nanoelectrodes with 20–30 nm diameter using a three-step process.[25] The first step is to establish a contact between a MWCNT and a tungsten probe or a carbon fiber inside a scanning electron microscope (SEM). The second step is to deposit a layer of HfO_2 *via* atomic layer deposition to insulate the entire probe. Then, the last step is to remove a part of the insulating layer at the MWCNT tip apex using a DC bias applied between the coated MWCNT and another tungsten probe. The authors show that the resulting CNT nanoelectrode exhibited similar electrochemical properties to the widely used carbon fiber probe in differential pulse voltammetry and cyclic voltammetry measurements.

Recently, the Gogotsi group developed a CNT-based endoscope for intracellular probing (Fig. 2).[26] In this method, a MWCNT is placed at the tip of a glass pipette using a flow-through technique. The inside of the glass pipette is coated with a conductive epoxy while the outside is coated with an insulator. As shown in Fig. 2B, these CNT-based endoscopes can penetrate the membrane of a cell without greatly disrupting the cellular structure owning to its small dimension and high mechanical strength. They can also be used to transport fluids and, additionally, can be manipulated magnetically if the CNT is filled with superparamagnetic NPs.

CNTs are also ideal materials to serve as imaging nanoelectrodes on AFM tips due to their well-defined geometry, nanometer-scale diameter, high aspect ratio, and outstanding electrical and mechanical properties.[27] The advantages of using SWCNT modified AFM probes include increased lateral resolution and damage resistance, the ability of probing narrow trench structures, and less difficulty of deconvoluting tip effects. Macpherson's group has demonstrated that low-resistance electrical contacts could be made by attaching a SWCNT to a metal-coated AFM tip using the "pick-up" method.[28] They have also shown that SWCNT–AFM tips could serve as templates for producing metal nanowire tips with diameters as small as 30 nm using sputter coating.[29] The resulting metal nanowire AFM tips can be conductive and durable enough for conducting and contact mode AFM imaging.

In summary, CNTs have been exploited in electrochemistry due to their unique properties. New fabrication methods and architectures are being produced to improve the performance of CNT-based nanoelectrodes. As a key material for nanoelec-

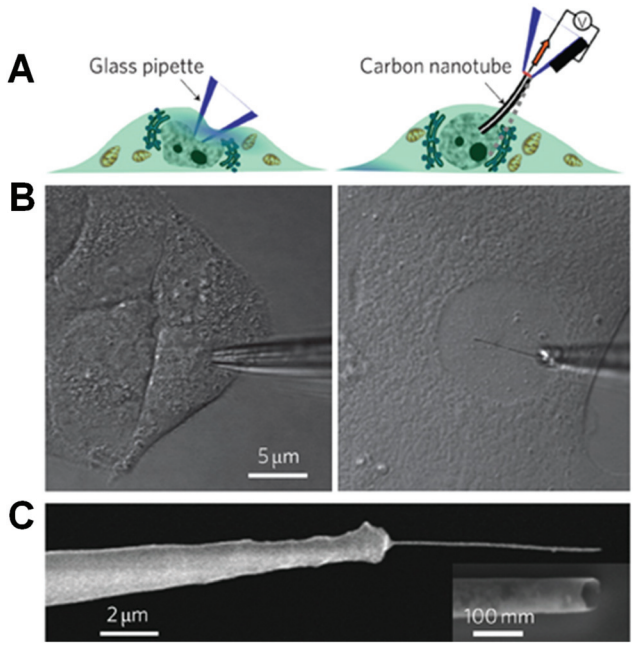

Fig. 2 (A) Schematic representation of a conventional glass pipette (left) and a nanotube endoscope (right) for intracellular probing. The nanotube endoscope could penetrate the membrane of a cell without greatly disrupting the cell. (B) A 1 μm glass pipette in a HeLa cell (left) and a 100 nm nanotube endoscope interrogating a primary rat hepatocyte nucleus. (C) SEM image of a nanotube endoscope with a 100 nm tip. The inset shows that the end of the nanotube remains open for fluid transfer. Adapted with permission from Singhal *et al.*[26] Copyright 2010 Nature Publishing Group.

trodes, we anticipate that CNTs will continue to be explored in this area in the future. The development and application of CNT-based nanoelectrodes will continue to benefit from the use of many microfabrication tools.

2.4 Carbon-filled glass/quartz nanopipettes

Bau's group developed carbon nanopipettes (CNPs) using an integrated fabrication protocol based on CVD.[30] At first the quartz capillaries were filled with a CVD catalyst solution, allowed to air dry, and then pulled with a laser puller. Carbon was deposited on the catalyzed surface by pyrolysis deposition with a methane/argon flow at over 800 °C, and only the carbon tip was exposed by etching the outside quartz. The carbon tip size could be further reduced by plasma oxidation. In this way they obtained an integrated nanoscale hollow carbon tip at the end of a carbon-coated quartz pipette. By varying the deposition conditions, the outer diameter of the carbon tip can be varied from tens to hundreds of nm with different lengths. Hollow carbon pipettes were used to deliver molecular species to a cell[31,32] and conduct intracellular electrochemical measurements.[32,33] The effect of changing fabrication conditions on the wall structure and surface chemistry of CNPs was also reported.[34] This fabrication procedure was later modified to fabricate solid-tipped CNPs. With longer carbon deposition time, the carbon tip could be sealed and the fabricated solid CNPs with 50–400 nm diameter were used to detect dopamine release in *Drosophila* larvae with high spatial resolution.[35]

Another fabrication method was developed by Gogotsi and coworkers.[36] This method is also based on pyrolysis decomposition but does not require CVD catalysts, and more importantly, enables batch production of smaller diameter (10–30 nm) carbon nanoelectrodes. First, quartz capillaries were pulled into nanopipettes using a laser puller. Then the pipette was inserted into another quartz capillary under Ar flow. A carbon-containing gas mixture such as methane and argon was injected. At high temperature, methane pyrolyzed and carbon was coated on both the inner and outer surfaces. Then, by wet etching, the quartz at the tip was removed to expose carbon. The quartz pipette orifice size and carbon layer thickness could be regulated to produce a tip as small as 10 nm. By controlling the gas composition and deposition time during pyrolysis, different kinds of CNPs have been fabricated. For example, longer deposition times produce thicker carbon layers and could result in a closed carbon channel with a nanometer-sized cavity at the end. This type of nanoelectrode can be utilized as a nanosampler[37] and a nanosensor after platinization.[38] The fabrication of disk-shaped carbon nanoelectrodes with radii of 5–200 nm was also reported.[39] The wet-etching step is skipped after carbon deposition in these later reports.

This approach has also been further developed to fabricate multifunctional nanoprobes using multi-barrel pipettes. For example, a fast and simple method was developed to fabricate double-barrel carbon nanoprobes based on this approach.[40] After a quartz theta capillary was pulled, one barrel was blocked temporarily with adhesive while carbon was deposited inside another barrel by CVD (Fig. 3). To increase the surface

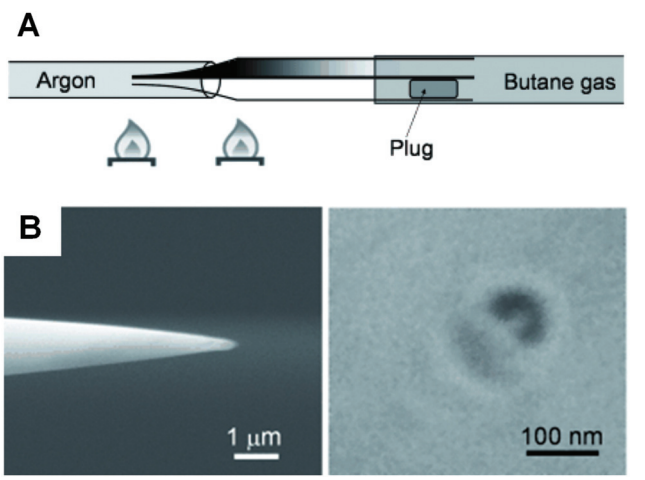

Fig. 3 (A) Schematic illustration of the fabrication of a double-barrel carbon nanoprobe (DBCNP) using the CVD method. A quartz theta capillary was pulled and one barrel was blocked while carbon was deposited inside another barrel. (B) Field emission scanning electron microscopy (FESEM) images of the side (left) and the top (right) of the DBCNP. Adapted with permission from Takahashi *et al.*[40] Copyright 2011 Wiley-VCH Verlag GmbH & Co. KGaA, Weinheim.

area of carbon, they coated carbon on the outside of the tip as well to produce a cylindrical tip. After the closed barrel was reopened and filled with electrolyte solution, this nanoprobe could be employed to carry out electrochemical and topographical imaging simultaneously in SECM-SICM. Further developments involved the fabrication of carbon–Ag/AgCl nanoprobes. Similarly, in a pulled theta pipette, one barrel is coated with carbon and another one is filled with electrolyte solution and an Ag/AgCl wire was inserted inside as a reference electrode to form a 2-electrode setup that can be used in a microdroplet.[41] Dual carbon electrodes for SECM were also produced by simply depositing carbon into both barrels.[2,42]

2.5 Tunneling nanoelectrodes based on immobilized single NPs

Bard and coworkers have demonstrated a unique method to fabricate a nanometer-sized electrode using a Pt UME and an immobilized metal NP.[43] This method deposits a layer of TiO_2 film onto a laser-pulled sub-micrometer-sized Pt UME and then captures a single Pt NP from solution *via* stochastic NP collision (Fig. 4). The electrodeposited TiO_2 film can block electron transfer to solution species but is also thin enough (1–2 nm) to allow electron tunneling to Pt NPs. Therefore, a TiO_2-covered Pt UME shows negligible current in a solution containing redox species, but gives a sudden current increase when a single Pt NP gets adsorbed to the UME, indicating the onset of electron tunneling from the UME to the attached Pt NP. The resulting electrode (Pt UME/TiO_2/Pt NP system) can be treated as a normal nanometer-sized Pt spherical electrode and can be used for steady-state measurements or probes in SECM. A quantitative model of electrochemistry has also been proposed to better understand this type of nanoelectrode.[44]

An alternative method for restoring electron transfer on a TiO_2-covered Pt UME is to electrodeposit a single Pt NP at the tunneling UME.[45] By recording current–time curves, the nucleation and growth of a stable single Pt NP can be monitored and the Pt NP radius can be estimated. These nanoelectrodes can be used to study fast kinetics of electron transfer reactions at the single Pt NPs.

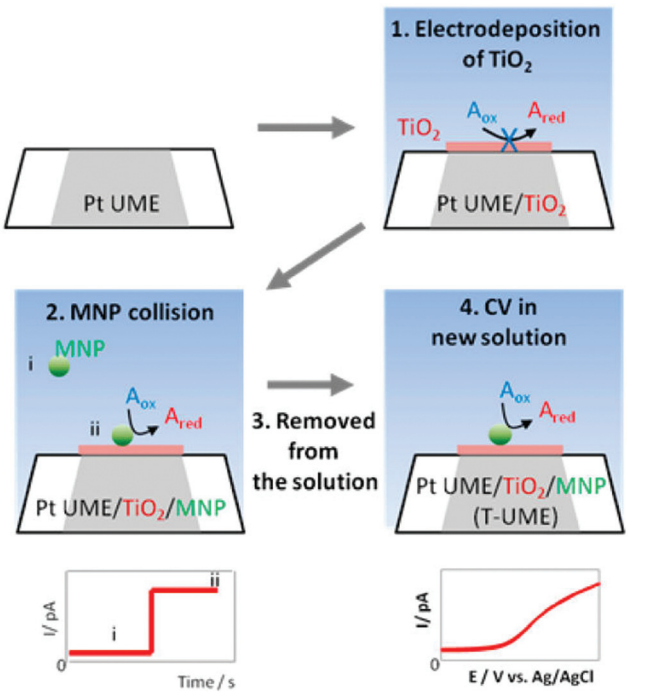

Fig. 4 Schematic illustration of the preparation of a Pt UME/TiO_2/Pt NP nanoelectrode (T-UME). A thin layer of TiO_2 was electrodeposited on a Pt UME to block electron transfer. When a single Pt NP collided and stuck to the UME, electron transfer to the solution species was restored. CVs could then be obtained using this T-UME in a new solution. Adapted with permission from Kim *et al.*[43] Copyright 2014 American Chemical Society.

2.6 Other fabrication techniques

Individual semiconducting boron nitride nanotubes (BNNT) can be employed to fabricate needle-like nanoprobes. Yu and coworkers attached BNNT onto a sharpened tungsten wire and then sputter-coated the BNNT with a thin layer (10–30 nm) of metal (Au, Ag, or Pt) followed by further insulation of the electrode by electropolymerization.[46] The ring-shaped active electrode area can be exposed by FIB cutting and the voltammetric responses can be recorded in redox solutions. Since the active electrode area is defined by the thickness of the metal coating, precise control over the active area is possible. Additionally, any conductive materials that can be sputter coated or electrochemically deposited can be fabricated into this type of nanoelectrode.

Shao and coworkers reported the fabrication of a special type of metal nanoelectrode by interfacial reactions.[47] This method uses a glass nanopipette to confine a limited space for the formation and self-assembly of metal NPs (Fig. 5A). The glass nanopipette is first filled with an aqueous metal precursor solution and then immersed into an organic phase containing a reductant. When the metal precursor meets the reductant at the liquid/liquid interface, metal NPs will form and self-assemble at the nanopipette tip. The metal NPs can densely block the pipette orifice and thus form a disk-shaped nanoelectrode. Using this method, Ag, Au, and Pt nanoelectrodes have been prepared and an Ag nanoelectrode has been successfully employed as a SECM probe.

Our group recently developed an approach to fabricate nanopipette-based electroplated nanoelectrodes (Fig. 5B).[48] In this approach, a laser-pulled quartz nanopipette serves as a template. The pipette tip is then immersed in a liquid gallium/indium alloy electrode for the electrochemical deposition of metal inside the pipette. Several different metals including Au, Pt, Ag, and Cu can be electroplated and FIB milled to expose the metal. This approach may be especially useful in fabricating nanoelectrodes for SECM, because it enables easy control over the RG ratio (the radius of the insulating sheath over the radius of the active electrode), a key geometric factor in high-resolution SECM.[49]

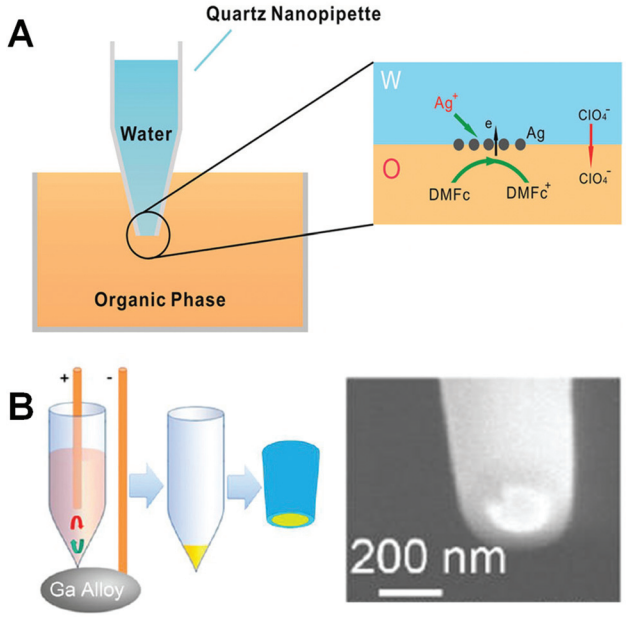

Fig. 5 (A) Schematic illustration of the formation and self-assembly of Ag NPs at the liquid/liquid interface at the nanopipette tip. A disk-shape nanoelectrode could be produced. Adapted with permission from Zhu *et al.*[47] Copyright 2014 American Chemical Society. (B) Nanopipette-based electroplated nanoelectrodes. Left: Schematic illustration of the fabrication of nanopipette-based electroplated nanoelectrodes. A quartz nanopipette tip was immersed in a liquid gallium/indium alloy electrode to electrochemically deposit metal inside the pipette. FIB milling was then used to expose the metal. Right: SEM image of a RG 2 gold nanoelectrode prepared using this method. Adapted with permission from Hao *et al.*[48] Copyright 2016 American Chemical Society.

3. New applications of nanoelectrodes

3.1 SECM and AFM/SICM–SECM

Since its development by Bard,[49] SECM has evolved into a well-established electroanalytical tool for measuring electrochemical information at an interface with exceedingly high spatial resolution. The central component of an SECM is a micro- or nanoelectrode which is positioned close to and scanned over the surface of a substrate of interest. The electrochemical signal of a redox mediator at the probe tip and/or the substrate is recorded to characterize processes and structural features of the substrate.

Nanoelectrodes have gained increasing popularity in high-resolution SECM due to their small size and fast response time. With a nanoelectrode, one can gain faster mass transport and higher spatial resolution and can image electrochemical reactions at individual NPs and study their reactivity. Recently, Mirkin's group employed Au nanoelectrodes as SECM probes to measure the kinetic parameters of several rapid heterogeneous electron transfer reactions by steady-state SECM voltammetry.[9] They varied the tip size and the tip–substrate distance to change the mass transfer rate. They also imaged individual spherical Au NPs of 10 to 20 nm and studied electron transfer and hydrogen evolution reaction at the surface with SECM.[50] This is a truly unprecedented spatial resolution which was achieved by reducing the size of the Pt nanoprobe to 3 nm. Very recently, they reported SECM imaging of Pd nanocubes with 14 nm edge length.[51] Their system could provide key information about the electrochemical and electrocatalytic properties of single NPs.[52]

Many groups have used SECM to study various biological systems due to the fact that it can quantitatively and locally detect chemical species *in situ* in a non-invasive manner.[53] With a nanoelectrode, there is insignificant disturbance of the tip redox reaction to the concentration profile of local chemical species, resulting in clear imaging. Matsue and coworkers studied the effect of tip reaction on SECM imaging of a single yeast cell.[54] They achieved quantitative imaging of a single yeast cell in generation–collection (GC) mode with a 199 nm Pt nanoelectrode. Interestingly, further decreasing the size of the Pt nanoelectrode did not yield higher spatial resolution. To obtain higher resolution, a better choice would be to incorporate distance control mechanisms such as shear force feedback into the SECM system.

Schuhmann's group is the first to adapt the shear force feedback mechanism in SECM.[55,56] Shear force techniques are now commonly utilized in a SECM system in order to achieve accurate control of the tip–substrate separation.[57,58] A shear force feedback system was used with an optical fiber-nanoelectrode probe to study the inner and outer functions of single living cells.[59] More recently, shear force-based SECM was also combined with an ion-selective nanoelectrode for simultaneous imaging of the topography and K^+ flux at the membrane filter and human embryonic kidney 293 cells.[60]

In order to simultaneously obtain both topographical and electrochemical information, significant progress has been made to combine different scanning probe microscopy techniques into SECM creating hybrid methods, such as AFM–SECM and SECM–SICM. In AFM, a sharp tip that is attached to a flexible cantilever is scanned across the sample and the force interactions between the tip and the sample surface can be measured at the nanometer scale. By combining AFM with SECM, the topographical information as well as the electrochemical activity of the sample surface could be collected, both with high lateral resolution. Macpherson and Unwin reported electrochemical and topographical measurements simultaneously with AFM–SECM for the first time.[61,62] In recent years, Demaille's group has published a series of papers in high-resolution AFM–SECM in molecule touching mode. In this mode, the nanoprobe is in contact with redox-tagged macromolecules electrochemically. Demaille and coworkers initially reported this configuration in 2006 and utilized it to show the dynamics of ferrocene-tagged polyethylene glycol (PEG) chains.[63] Later, this configuration was also applied to study the dynamics of DNA chains.[64] Due to the capability for dual measurement and high spatial resolution, topographical and electrochemical mapping of single gold nanoparticles (~20 nm) modified with redox-labeled PEG chains could be achieved.[65] They also studied the possibility of locating

antibodies with redox PEG chains with the same technique.[66] More recently, they mapped protein distribution on virus particles both statistically and spatially, which is very interesting because it extended the potential of AFM–SECM to viral nanotechnology.[67]

There are also advances in developing proper nanoprobes for AFM–SECM in order to achieve high spatial resolution. Macpherson and coworkers reported a new method to fabricate nanoprobes with well-controlled size and geometry by forming metal nanowires while using single-walled carbon nanotubes as templates, followed by insulation and cutting.[68] Baker's group formed a thin (less than 400 nm) insulation layer on commercial AFM probes by parylene deposition.[69] After mechanical abrasion, the probes could be used to map the diffusion of $Ru(NH)_6^{3+}$ across a porous membrane. Richter's group described a batch fabrication technique from the wafer level by combining FIB and wet chemical etching.[70] The conical nanoprobes were applied to map heterogeneous graphene and graphite surfaces.

SICM is a unique scanning probe technique based on the use of an electrolyte-filled glass/quartz nanopipette as a probe. The ionic current flowing through the pipette orifice is strongly dependent on the tip–substrate distance and can be used as a feedback signal for distance control. SICM is particularly suitable for imaging soft biological structures with spatial resolutions better than 100 nm. However, little or no chemical information is obtained from SICM scanning. Korchev and coworkers have greatly contributed to the recent improvements in SICM for studying biological processes in living cells with high spatial and temporal resolutions.[71,72] More recently they have investigated the quantitative delivery of molecules to the surface of living cells,[73] which allows for functional imaging of single ion channels and receptors. Matsue and coworkers used SICM to evaluate an unlabeled secretory protein in living cells.[74] Unwin's group developed a new function of SICM and demonstrated how it can map spatial distributions of ionic fluxes due to electrochemical reactions near active sites.[75] They also developed a new approach to characterize the surface charge of a nanopipette and facilitated quantitative surface charge imaging in SICM.[76]

One of the key challenges in SECM–SICM is the preparation of proper probes with small and controlled geometry and functionality. Several notable efforts have been made in recent years to develop proper SECM–SICM nanoprobes. Hersam's group successfully combined SECM electrodes with SICM pipettes by coating nanopipettes with Au, followed by tip insulation and exposure.[77] These probes have later been applied for the simultaneous topography and electrochemical imaging of enzymes and single living cells.[78] However, this method still requires an additional FIB milling step to expose the probe. Recently a quick and simple method for fabricating double-barrel carbon nanoprobes (DBCNPs) for SECM–SICM has been developed.[40] The details of the fabrication have been given in the section New fabrication methods. This probe was later employed to image the electroactive features at a 100–150 nm scale and demonstrate the oxygen reduction reaction (ORR)

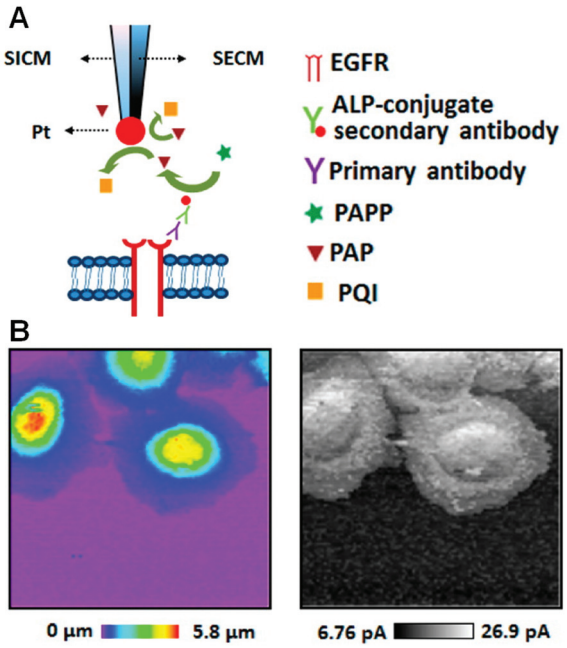

Fig. 6 (A) Schematic illustration of the electrochemically sensitive high-resolution imaging of EGFR proteins using a double barrel SECM–SICM probe with deposited Pt. (B) Topographic (left) and electrochemical (right) images of A431 cells obtained using Pt deposited probes. The scanned area is 75 × 75 μm. Adapted with permission from Sen *et al.*[80] Copyright 2015 American Chemical Society.

activity at the single NP level for the first time.[79] More recently, Matsue's group[80] and Wain's group[81] further improved the electrochemical sensitivity of DBCNP by Pt deposition on carbon to image immunocytochemically stained epidermal growth factor receptor (EGFR) proteins on A431 cells (Fig. 6) and hydrogen peroxide generation at individual Au NPs, respectively. Iridium oxide has also been deposited on carbon to obtain a pH-SICM probe, which enabled simultaneous pH and topography mapping.[82]

3.2 The use of nanoelectrodes for single-cell studies

The ability to electrochemically probe tight spaces is important for better understanding the biological functions of single living cells. One straightforward example has been the use of a nanoelectrode to monitor cell exocytosis with high spatial resolution.[83,84] A nanoelectrode can also be inserted inside a cell or tissue without disturbing the cellular function.[85] Carbon has been shown to be an excellent electrode material for cell detection because of its high stability and relatively large potential window. Carbon-fiber electrodes can be etched or flame polished to expose an ultrasharp conical tip and be inserted into tissue or a cell without causing significant damage. Huang and coworkers reported the fabrication of an etched carbon-fiber nanoelectrode with the proper size to slip into synaptic clefts without damaging local structures.[86,87] This allows the direct measurement of exocytosis inside single synapses. Ewing's group implanted a carbon-fiber nanotip into

living PC12 cells and measured the total content of catecholamine in single vesicles as vesicles were adsorbed onto the electrode.[88] They found that only a part of the catecholamine content was released during exocytosis, indicating the necessity of investigating single vesicles before they are released.

The carbon nanopipette electrodes are another promising tool in single-cell analysis because they can be batch-fabricated with a small and controllable size. They are more rigid than carbon-fiber nanoelectrodes due to the use of quartz as an insulation layer. It has been shown that closed CNPs could be implanted into dopaminergic centers of *Drosophila* brain for dopamine detection.[35] Another advantage of CNPs is their ability to be extended to multifunctional nanoprobes. For example, a double-barrel nanopipette with a carbon coating in one barrel and a Ag/AgCl wire in the other electrolyte-filled barrel formed a two-electrode circuit to detect the alkaline phosphatase activity of HeLa cells in a single droplet (Fig. 7).[41] Zhang *et al.* deposited carbon into double-barrel nanopipettes and fabricated nanometric field-effect transistor sensors on the tip of the dual carbon nanoelectrodes.[89] With further modification they used this nanosensor to monitor pH changes and ATP gradient around living cells in three dimensions.

Hollow CNPs can facilitate simultaneous intracellular injection and detection. In the past few years, Bau's group contributed to the development of a carbon nanopipette (CNP) in cell detection.[30–32] In a later study, they penetrated a CNP into single adherent human osteosarcoma cells and nuclei and correlated CNP impedance with cell penetration depth. Such experiments may enable position control of nanoelectrodes for intracellular probing in the future.[33]

Nanoelectrodes with modifications are also employed to detect reactive oxygen and nitrogen species in tissues and cells.[39,90,91] For example, a collaborative research between Amatore and Mirkin has used a platinized nanoelectrode under AFM control to detect reactive oxygen and nitrogen species inside murine macrophages.[91] More recently, Korchev's group fabricated disk-shaped carbon nanoelectrodes and functionalized them with platinum.[39] The carbon nanoelectrode had a smaller outer diameter and was used to monitor oxygen concentration in a brain slice and melanoma cells at the single-cell level.

3.3 Single-enzyme electrochemistry

Direct electrochemical detection of single enzymatic molecules is challenging due to the low turnover frequency and, thus, extremely low faradaic current signal. A dramatic improvement in signal amplification must be achieved and the background signal must be suppressed for this type of measurement. Nanoelectrodes have a small background current due to the small surface area and therefore can be used to detect a small number of molecules. Using lithographically fabricated polymyxin-pretreated Au nanoelectrodes, Lemay and coworkers have demonstrated protein film voltammetry (PFV) measurements on less than 50 enzyme molecules (*Av* H_2ase).[92] Polymyxin was used to immobilize a submonolayer of *Av* H_2ase,[93] an enzyme that reversibly interconverts molecular hydrogen into protons and electrons. The signal amplification comes from the extremely high turnover rate (~1500 to 9000 s^{-1}) of *Av* H_2ase catalyzing H_2 oxidation.

More recently, Lemay's group has demonstrated the ultrahigh sensitivity of nanogap devices for detecting single redox-active molecules.[94–96] The devices consist of two electrodes that are separated by a short distance created in a nanochannel. The top and bottom electrodes are biased at oxidizing and reducing potentials, respectively, to enable redox cycling. The redox-active molecules are thus repeatedly oxidized and reduced at the two electrodes, resulting in a detectable current signal. The authors observed anticorrelated step-like events in the current, corresponding to a single molecule entering and exiting the nanogap. The small gap size and minimized dead volume greatly amplified the current signal and reduced the number of redox-active molecules in the nanochannel, making this a robust technique for detecting individual redox molecules. In another report,[97] they further implemented this approach by integrating enzymatic recognition with signal transduction in a femtoliter-scale volume. In this report, tyrosinase is locally immobilized on the Au electrodes in a microfabricated nanochannel to transform substrate molecules that are not redox-active into redox-active enzymatic product

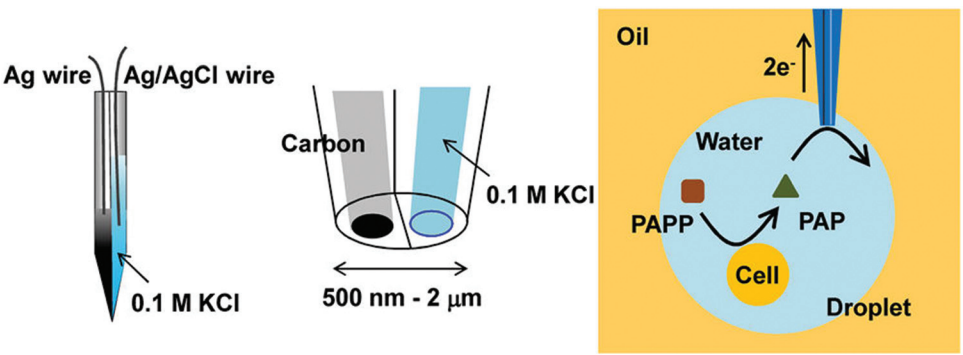

Fig. 7 Schematic illustration of the electrochemical detection of the alkaline phosphatase (ALP) activity of a cell in a single droplet using a carbon–Ag/AgCl probe. ALP catalyzed the hydrolysis of *p*-aminophenyl phosphate (PAPP) to *p*-aminophenol (PAP) that could be oxidized at the probe. Adapted with permission from Ino *et al.*[41] Copyright 2013 American Chemical Society.

molecules. The product molecules are then detected inside the nanochannel by redox cycling. It is anticipated that further improvement of this approach would lead to an electrochemical study of enzyme kinetics at a single-molecule level.[98]

Single enzyme molecules can also be electrochemically detected on a nanoelectrode based on collision induced adsorption. Bard's group demonstrated the detection of electrochemically inactive single bio-macromolecules (enzymes, antibodies, and DNA) by current blockage of a redox-active species in solution.[99] Using Pt disk nanoelectrodes with radii between 80 and 150 nm and potassium ferrocyanide, a steady-state oxidation current was generated. Adsorption of an electrochemically inactive object onto the Pt electrode blocks a part of the oxidation current of ferrocyanide, leading to a stair-case-shaped current signal. Information about the adsorbed molecules such as concentration and size distribution could then be extracted from the recorded *i*–*t* curves. In this method, a small electrode and a high concentration of redox-active species are necessary in order to gain sufficient current amplification and observe discrete adsorption events.

Zhan and coworkers recently presented another mechanism to detect single-molecule catalysis of redox enzymes using collision.[100] They first modified a 12 nm radius Au nanoelectrode with a lipid bilayer membrane and then recorded amperometric curves to detect collision events of electrocatalytic reduction of hydrogen peroxide by individual horseradish peroxidase (HRP) molecules. Different from the blocking effect described by Bard[99] mentioned above, the enzymes were electrocatalytically active and the current amplification came from the high turnover coefficient.

3.4 Single-NP electrochemistry

Metal NPs have found wide applications in sensing, biotechnology, catalysis, and electrocatalysis due to their unique catalytic, optical, and biochemical properties.[101–103] Extensive studies have been conducted on metal NPs to understand the structure–function relationship and single NP studies are preferred to avoid ensemble averaging.[104–106] Nanoelectrodes are particularly suitable for studying single NPs electrochemically. Due to its small size, a single NP could be either attached to or grown on a nanoelectrode.

Our group has reported a method to chemically immobilize a single Au NP at the surface of a Pt disk nanoelectrode.[107] In our method, a laser-pulled Pt nanoelectrode was modified by a linker molecule, (3-aminopropyl)trimethoxysilane. Then, a single Au NP with a diameter of 10–30 nm was immobilized at the amino-terminated Pt surface *via* electrostatic interaction. TEM images were obtained to confirm the attachment of the Au NP and to measure the electrode size. Voltammetric responses of the Au single NP electrode assembly (SNPE) in H_2SO_4 further confirmed the existence of the Au NP. Steady-state cyclic voltammetry in solutions containing $Fe(CN)_6^{3-}$ and $Ru(NH_3)_6^{3+}$ showed that electron transfer from the Pt nanoelectrode to the redox molecules was greatly enhanced due to the attachment of the Au NP and the magnitude of the steady-state current was dependent on the size of the Au NP. The size-dependent catalytic activity towards oxygen reduction reaction (ORR) in a KOH solution was also revealed using the same Pt nanoelectrode immobilized with single Au NPs with different sizes. Using this method, the effects of NP size and shape on electrocatalytic activities could be studied. Similarly, Sun and coworkers studied the electrochemical stability of single Au NPs directly adsorbed on a Pt nanoelectrode.[108] They have shown that smaller Au NPs were harder to oxidize.

Mirkin and coworkers have immobilized single Au NPs onto carbon nanoelectrodes to study the catalytic activities of single Au NPs.[109] The carbon nanoelectrodes were fabricated by using CVD of carbon inside a nanopipette and the electrode size was smaller than the size of a single Au NP to ensure that only one NP was attached to the nanoelectrode surface (Fig. 8A and B). Three methods were used to immobilize single Au NPs: direct adsorption, electrostatic attachment through a polyphenylene film, and covalent bonding through an electrochemically reduced polyphenylene film. Compared to the catalytic activity at a directly adsorbed Au NP, the catalytic activity towards the hydrogen evolution reaction (HER) was observed to be lower at an electrostatically attached Au NP. This is probably due to the insulating effects of the polyphenylene film.

Besides attachment, single NPs can also be deposited onto a nanoelectrode. Sun *et al.* deposited a single Au NP on the surface of a Pt nanoelectrode under open circuit potential in a solution containing 1% $HAuCl_4$.[110] Different from bulk gold, the spontaneously formed Au NP showed stability in acidic solution during voltammetric scanning. Schuhmann's group have deposited single $Ni(OH)_2$ NPs on carbon nanoelectrodes

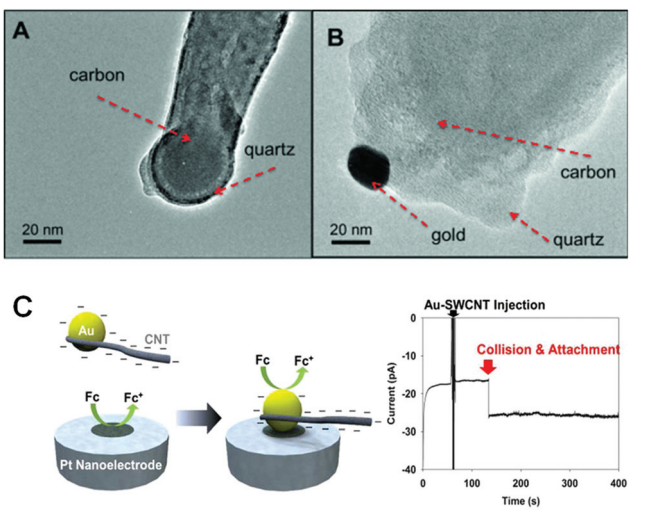

Fig. 8 (A) TEM image of a pulled quartz nanopipette filled with carbon. (B) TEM image of a 20 nm Au NP attached to a carbon nanoelectrode tip. (A) and (B) are adapted with permission from Yu *et al.*[109] Copyright 2015 Wiley-VCH Verlag GmbH & Co. KGaA, Weinheim. (C) Schematic illustration of the collision of a carbon nanotube (CNT)-modified Au NP at a Pt nanoelectrode (left). Upon CNT-modified Au NP attachment, an increase in current could be observed in the amperometric curve due to the increase in electrode area (right). (C) and (D) are adapted with permission from Park *et al.*[114] Copyright 2013 American Chemical Society.

and investigated the electrocatalytic activity of the single NPs for the oxygen evolution reaction (OER).[111] The size-dependent catalytic turnover rate for OER was obtained at individual Ni $(OH)_2$ NPs and it has been found that the OER activity was independent of the NP size.

Stochastic NP collision is a simple yet powerful method to study single NP catalysis.[104] First reported by Bard's group,[112,113] this method involves free diffusing catalytic NPs, an inert UME, and inner-sphere redox molecules. Collision and adsorption of a NP on the UME surface led to a transient current increase due to the catalytic effects of the NP. Bard and coworkers recently employed nanometer-sized Pt electrodes to detect collisions of Au NP-decorated single wall carbon nanotubes (Au-SWCNTs).[114] Due to the extremely small size, the Pt nanoelectrodes could be used to observe the current increase resulting from the increase in electrode area upon Au-SWCNT attachment (Fig. 8C). This approach extended the NP collision method to the use of nanoelectrodes and outer-sphere electron-transfer reactions.

3.5 Formation and electrochemistry of individual nanobubbles

Surface nanobubbles have attracted significant research interest in the past two decades due to their important roles in altering interfacial properties at the nanoscale.[115] Nanoelectrodes provide a unique platform for the generation and study of single nanobubbles. White's group has demonstrated the electrogeneration of single nanobubbles at Pt nanodisk electrodes using proton reduction (Fig. 9).[116] By scanning a Pt nanodisk electrode in 0.5 M H_2SO_4, current from H^+ reduction and H_2 generation increased initially but dropped prior to reaching the diffusion-limited steady-state current, indicating the formation of a single nanobubble covering the majority of the electrode surface. Interestingly, a residual current was obtained which suggested that the nanobubble formed could not cover the whole active area of the nanoelectrode. It also indicated that the exposed electrode area could continue to generate molecular hydrogen to balance the diffusion of H_2 from the nanobubble, extending the nanobubble lifetime. Additionally, the sudden current decrease could only be observed when the size of the Pt nanoelectrode was below 100 nm. This suggests that an ultrafast mass transfer rate is necessary to reach a critical saturation point for nanobubble formation. Nanoelectrodes are particularly attractive for bubble formation because the mass transfer rate on a nanoelectrode is inversely proportional to its radius. Finite-element simulation was conducted and showed that the H_2 concentration exceeded the saturation H_2 concentration near the electrode surface.

In another report, White's group further studied the effect of surfactants on bubble nucleation and stability.[117] Cyclic voltammograms have shown that the addition of surfactant molecules decreased the nanobubble peak current, reduced the residual current, and shifted the potentials corresponding to bubble nucleation cathodically. The decrease of the peak current and the residual current could be explained by the decrease of the surface tension of the solution due to the presence of surfactants. Also, surfactant molecules could hinder the hydrogen gas diffusion from the nanobubble, leading to a smaller residual current needed for H_2 electrogeneration. The shifted bubble nucleation potential was probably due to the adsorption of surfactants at the electrode surface, hindering electron transfer.

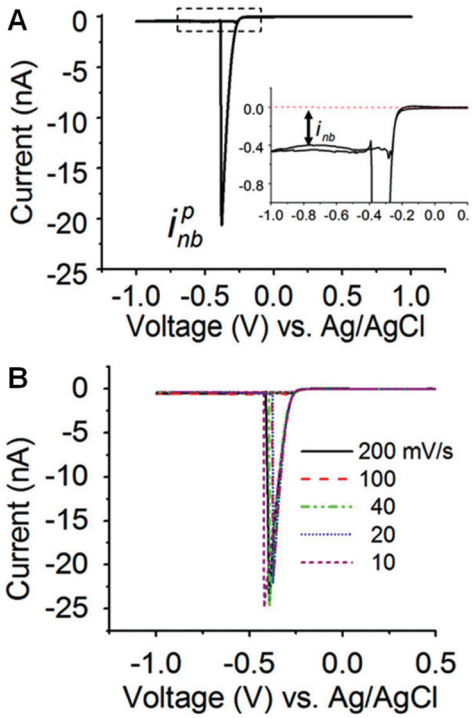

Fig. 9 (A) Cyclic voltammogram of a 27 nm-radius Pt electrode in a 0.5 M H_2SO_4 solution at a scan rate of 100 mV s^{-1}. As the potential is scanned cathodically, the current firstly increased due to proton reduction and then suddenly dropped at ~−0.4 V due to the nucleation and quick growth of a hydrogen bubble at the electrode surface. The peak current is labeled i^p_{nb}. The inset shows ~−0.4 nA of a residual current after the formation of a nanobubble. (B) Cyclic voltammograms of the same 27 nm-radius Pt electrode recorded in the same H_2SO_4 solution at different scan rates. Adapted with permission from Luo *et al.*[116] Copyright 2013 American Chemical Society.

Besides using a Pt disk nanoelectrode to study H_2 nanobubbles, White's group studied individual N_2 nanobubbles *via* electro-oxidation of hydrazine using Pt disk nanoelectrodes and observed a similar nanobubble peak current and residual current.[118–120] They have also reported the use of a recessed Pt nanopore electrode to generate single hydrogen nanobubbles.[121] Due to the trapping effect of the recessed cavity, a H_2 oxidation peak could be observed on the reverse voltammetric scan.

3.6 Other applications

Nanoelectrodes can be used to study single active surface sites for metal nucleation using AFM imaging. Mirkin and coworkers have imaged the surface of laser-pulled disk-shaped nanoelectrodes using AFM and have gained detailed information

about the electrode surface and geometry.[122] Mirkin's group then used AFM to investigate the nucleation and growth of single silver crystals on the surface of Pt nanoelectrodes.[123] They have found that only one nucleation site existed on the surface of a 50 nm Pt electrode while two active sites existed on the surface of a 190 nm electrode. As such, the combined use of nanoelectrodes and AFM allowed them to measure nucleation/growth kinetics on active surface sites, which is fundamentally important in the initial stages of metal electrodeposition.

Our group recently studied the formation and quick growth of thick platinum oxide films to understand oxidation behaviors of Pt catalysts using a Pt nanoelectrode.[124] In this study, Pt nanoelectrodes were used as model electrocatalysts and were held at relatively low anodic potentials to form thick Pt oxide films. Using SEM and steady-state cyclic voltammetry, it was observed that the Pt oxide film protruded out of the glass insulator due to increased volume and was structurally irreversible. An increased steady-state current after the oxidation and reduction process provided quantitative information about the final recessed depth of Pt and an oxide growth rate of ~1.2 nm min^{-1} could be estimated. Pt nanoelectrodes used in this study had the advantages of having nanoscale dimensions and better control of the size and morphology of the electrocatalysts.

Using laser-pulled Pt nanoelectrodes covered with different thicknesses of borosilicate glass, Mirkin and coworkers have found that water molecules can diffuse to the Pt surface through nanometer-thick layers of dry glass and be electrochemically oxidized/reduced at the Pt surface.[125] If soaked for several hours in acidic aqueous solution, the nanometer-thick glass sheath could swell and form a hydrogel surface layer, allowing electrochemical oxidation/reduction processes of other redox couples such as $Ru(NH_3)_6^{3+/2+}$ to happen at the Pt/hydrogel interface. These thin-glass covered Pt nanoelectrodes can potentially serve as all-solid-state pH nanoprobes and are suitable for experiments in small volumes due to their small size.

4. Conclusions and perspectives

In summary, nanoelectrodes continue to be the tool of central importance in modern electrochemistry and electroanalytical research. Their small size, low noise, and fast response make them uniquely suitable for numerous applications, such as the study of single molecules/NPs, sensing inside a chemical synapse and single biological cells, mapping the reactivity of single catalytic NPs at ultrahigh spatial resolution, and generating and studying individual nanobubbles. New and exciting applications of nanoelectrodes are anticipated to emerge along with advanced electrode fabrication methods. Bench-top methods for nanoelectrode fabrication will continue to be used in future research. However, future nanoelectrodes will likely be mass prepared with microfabrication methods, so researchers can spend less effort on electrode preparation and focus more on the scientific problems. We believe that nanoelectrodes will find more use in several areas in the near future including single molecule electrochemistry, neurochemical analysis of single cells, and ultrahigh-resolution chemical imaging.

Acknowledgements

We are grateful for the financial support from the National Science Foundation (CHE-1505897), the National Institutes of Health (GM101133), the AFOSR MURI (FA9550-14-1-0003), and the U.S. Defense Threat Reduction Agency (contract no. HDTRA1-11-1-0005). We also thank Peter Defnet for a careful reading of the manuscript.

References

1 S. M. Oja, M. Wood and B. Zhang, *Anal. Chem.*, 2013, **85**, 473–486.
2 R. W. Murray, *Chem. Rev.*, 2008, **108**, 2688–2720.
3 J. T. Cox and B. Zhang, *Annu. Rev. Anal. Chem.*, 2012, **5**, 253–272.
4 S. Chen and Y. Liu, *Phys. Chem. Chem. Phys.*, 2014, **16**, 635–652.
5 J. Clausmeyer and W. Schuhmann, *TrAC, Trends Anal. Chem.*, 2016, **79**, 46–59.
6 Y. Shao, M. V. Mirkin, G. Fish, S. Kokotov, D. Palanker and A. Lewis, *Anal. Chem.*, 1997, **69**, 1627–1634.
7 B. B. Katemann and W. Schuhmann, *Electroanalysis*, 2002, **14**, 22–28.
8 B. Zhang, J. Galusha, P. G. Shiozawa, G. Wang, A. J. Bergren, R. M. Jones, R. J. White, E. N. Ervin, C. C. Cauley and H. S. White, *Anal. Chem.*, 2007, **79**, 4778–4787.
9 J. Velmurugan, P. Sun and M. V. Mirkin, *J. Phys. Chem. C*, 2009, **113**, 459–464.
10 J.-M. Noël, J. Velmurugan, E. Gökmeşe and M. V. Mirkin, *J. Solid State Electrochem.*, 2012, **17**, 385–389.
11 M. A. Mezour, M. Morin and J. Mauzeroll, *Anal. Chem.*, 2011, **83**, 2378–2382.
12 J. Velmurugan and M. V. Mirkin, *ChemPhysChem*, 2010, **11**, 3011–3017.
13 L. Danis, S. M. Gateman, M. E. Snowden, I. C. Halalay, J. Y. Howe and J. Mauzeroll, *Electrochim. Acta*, 2015, **162**, 169–175.
14 Y. Zhang, S. Xu, Y. Qian, X. Yang and Y. Li, *RSC Adv.*, 2015, **5**, 77248–77254.
15 Y. Li, D. Bergman and B. Zhang, *Anal. Chem.*, 2009, **81**, 5496–5502.
16 R. Chen, K. Hu, Y. Yu, M. V. Mirkin and S. Amemiya, *J. Electrochem. Soc.*, 2016, **163**, H3032–H3037.
17 C. Yang and P. Sun, *Anal. Chem.*, 2009, **81**, 7496–7500.
18 T. W. Johnson, Z. J. Lapin, R. Beams, N. C. Lindquist, S. G. Rodrigo, L. Novotny and S.-H. Oh, *ACS Nano*, 2012, **6**, 9168–9174.

19 J. Jose, S. Kress, A. Barik, L. M. Otto, J. Shaver, T. W. Johnson, Z. J. Lapin, P. Bharadwaj, L. Novotny and S.-H. Oh, *ACS Photonics*, 2014, **1**, 464–470.
20 H. Im and S.-H. Oh, *Small*, 2014, **10**, 680–684.
21 E. Katz and I. Willner, *ChemPhysChem*, 2004, **5**, 1084–1104.
22 C. Dekker, *Phys. Today*, 1999, **52**, 22.
23 I. Heller, J. Kong, H. A. Heering, K. A. Williams, S. G. Lemay and C. Dekker, *Nano Lett.*, 2005, **5**, 137–142.
24 I. Heller, J. Kong, K. A. Williams, C. Dekker and S. G. Lemay, *J. Am. Chem. Soc.*, 2006, **128**, 7353–7359.
25 J. Shen, W. Wang, Q. Chen, M. Wang, S. Xu, Y. Zhou and X.-X. Zhang, *Nanotechnology*, 2009, **20**, 245307.
26 R. Singhal, Z. Orynbayeva, R. V. Kalyana Sundaram, J. J. Niu, S. Bhattacharyya, E. A. Vitol, M. G. Schrlau, E. S. Papazoglou, G. Friedman and Y. Gogotsi, *Nat. Nanotechnol.*, 2011, **6**, 57–64.
27 N. R. Wilson and J. V. Macpherson, *Nat. Nanotechnol.*, 2009, **4**, 483–491.
28 N. R. Wilson, D. H. Cobden and J. V. Macpherson, *J. Phys. Chem. B*, 2002, **106**, 13102–13105.
29 N. R. Wilson and J. V. Macpherson, *Nano Lett.*, 2003, **3**, 1365–1369.
30 M. G. Schrlau, E. M. Falls, B. L. Ziober and H. H. Bau, *Nanotechnology*, 2008, **19**, 015101.
31 M. G. Schrlau, E. Brailoiu, S. Patel, Y. Gogotsi, N. J. Dun and H. H. Bau, *Nanotechnology*, 2008, **19**, 325102.
32 M. G. Schrlau, N. J. Dun and H. H. Bau, *ACS Nano*, 2009, **3**, 563–568.
33 S. E. Anderson and H. H. Bau, *Nanotechnology*, 2015, **26**, 185101.
34 E. A. Vitol, M. G. Schrlau, S. Bhattacharyya, P. Ducheyne, H. H. Bau, G. Friedman and Y. Gogotsi, *Chem. Vap. Deposition*, 2009, **15**, 204–208.
35 H. R. Rees, S. E. Anderson, E. Privman, H. H. Bau and B. J. Venton, *Anal. Chem.*, 2015, **87**, 3849–3855.
36 R. Singhal, S. Bhattacharyya, Z. Orynbayeva, E. Vitol, G. Friedman and Y. Gogotsi, *Nanotechnology*, 2010, **21**, 015304.
37 Y. Yu, J.-M. Noël, M. V. Mirkin, Y. Gao, O. Mashtalir, G. Friedman and Y. Gogotsi, *Anal. Chem.*, 2014, **86**, 3365–3372.
38 K. Hu, Y. Gao, Y. Wang, Y. Yu, X. Zhao, S. A. Rotenberg, E. Gökmeşe, M. V. Mirkin, G. Friedman and Y. Gogotsi, *J. Solid State Electrochem.*, 2013, **17**, 2971–2977.
39 P. Actis, S. Tokar, J. Clausmeyer, B. Babakinejad, S. Mikhaleva, R. Cornut, Y. Takahashi, A. López Córdoba, P. Novak, A. I. Shevchuck, J. A. Dougan, S. G. Kazarian, P. V. Gorelkin, A. S. Erofeev, I. V. Yaminsky, P. R. Unwin, W. Schuhmann, D. Klenerman, D. A. Rusakov, E. V. Sviderskaya and Y. E. Korchev, *ACS Nano*, 2014, **8**, 875–884.
40 Y. Takahashi, A. I. Shevchuk, P. Novak, Y. Zhang, N. Ebejer, J. V. Macpherson, P. R. Unwin, A. J. Pollard, D. Roy, C. A. Clifford, H. Shiku, T. Matsue, D. Klenerman and Y. E. Korchev, *Angew. Chem., Int. Ed.*, 2011, **50**, 9638–9642.
41 K. Ino, K. Ono, T. Arai, Y. Takahashi, H. Shiku and T. Matsue, *Anal. Chem.*, 2013, **85**, 3832–3835.
42 K. McKelvey, B. P. Nadappuram, P. Actis, Y. Takahashi, Y. E. Korchev, T. Matsue, C. Robinson and P. R. Unwin, *Anal. Chem.*, 2013, **85**, 7519–7526.
43 J. Kim, B. K. Kim, S. K. Cho and A. J. Bard, *J. Am. Chem. Soc.*, 2014, **136**, 8173–8176.
44 C. M. Hill, J. Kim and A. J. Bard, *J. Am. Chem. Soc.*, 2015, **137**, 11321–11326.
45 J. Kim and A. J. Bard, *J. Am. Chem. Soc.*, 2016, **138**, 975–979.
46 K. Yum, H. N. Cho, J. Hu and M.-F. Yu, *ACS Nano*, 2007, **1**, 440–448.
47 X. Zhu, Y. Qiao, X. Zhang, S. Zhang, X. Yin, J. Gu, Y. Chen, Z. Zhu, M. Li and Y. Shao, *Anal. Chem.*, 2014, **86**, 7001–7008.
48 R. Hao and B. Zhang, *Anal. Chem.*, 2016, **88**, 614–620.
49 A. J. Bard, F. R. F. Fan, J. Kwak and O. Lev, *Anal. Chem.*, 1989, **61**, 132–138.
50 T. Sun, Y. Yu, B. J. Zacher and M. V. Mirkin, *Angew. Chem., Int. Ed.*, 2014, **53**, 14120–14123.
51 P.-Y. Blanchard, T. Sun, Y. Yu, Z. Wei, H. Matsui and M. V. Mirkin, *Langmuir*, 2016, **32**, 2500–2508.
52 Y. Yu, T. Sun and M. V. Mirkin, *Anal. Chem.*, 2015, **87**, 7446–7453.
53 P. Sun, F. O. Laforge, T. P. Abeyweera, S. A. Rotenberg, J. Carpino and M. V. Mirkin, *Proc. Natl. Acad. Sci. U. S. A.*, 2008, **105**, 443–448.
54 K. Nagamine, Y. Takahashi, K. Ino, H. Shiku and T. Matsue, *Electroanalysis*, 2011, **23**, 1168–1174.
55 M. Ludwig, C. Kranz, W. Schuhmann and H. E. Gaub, *Rev. Sci. Instrum.*, 1995, **66**, 2857.
56 A. Hengstenberg, C. Kranz and W. Schuhmann, *Chem. – Eur. J.*, 2000, **6**, 1547–1554.
57 B. Ballesteros Katemann, A. Schulte and W. Schuhmann, *Chem. – Eur. J.*, 2003, **9**, 2025–2033.
58 B. Ballesteros Katemann, A. Schulte and W. Schuhmann, *Electroanalysis*, 2004, **16**, 60–65.
59 Y. Takahashi, H. Shiku, T. Murata, T. Yasukawa and T. Matsue, *Anal. Chem.*, 2009, **81**, 9674–9681.
60 H. Yamada, D. Haraguchi and K. Yasunaga, *Anal. Chem.*, 2014, **86**, 8547–8552.
61 J. V. Macpherson and P. R. Unwin, *Anal. Chem.*, 2000, **72**, 276–285.
62 J. V. Macpherson and P. R. Unwin, *Anal. Chem.*, 2001, **73**, 550–557.
63 J. Abbou, A. Anne and C. Demaille, *J. Phys. Chem. B*, 2006, **110**, 22664–22675.
64 K. Wang, C. Goyer, A. Anne and C. Demaille, *J. Phys. Chem. B*, 2007, **111**, 6051–6058.
65 K. Huang, A. Anne, M. A. Bahri and C. Demaille, *ACS Nano*, 2013, **7**, 4151–4163.
66 A. Anne, A. Chovin, C. Demaille and M. Lafouresse, *Anal. Chem.*, 2011, **83**, 7924–7932.
67 L. Nault, C. Taofifenua, A. Anne, A. Chovin, C. Demaille, J. Besong-Ndika, D. Cardinale, N. Carette, T. Michon and J. Walter, *ACS Nano*, 2015, **9**, 4911–4924.

68 D. P. Burt, N. R. Wilson, J. M. R. Weaver, P. S. Dobson and J. V. Macpherson, *Nano Lett.*, 2005, **5**, 639–643.
69 M. A. Derylo, K. C. Morton and L. A. Baker, *Langmuir*, 2011, **27**, 13925–13930.
70 A. J. Wain, A. J. Pollard and C. Richter, *Anal. Chem.*, 2014, **86**, 5143–5149.
71 P. Novak, C. Li, A. I. Shevchuk, R. Stepanyan, M. Caldwell, S. Hughes, T. G. Smart, J. Gorelik, V. P. Ostanin, M. J. Lab, G. W. J. Moss, G. I. Frolenkov, D. Klenerman and Y. E. Korchev, *Nat. Methods*, 2009, **6**, 279–281.
72 A. I. Shevchuk, G. I. Frolenkov, D. Sánchez, P. S. James, N. Freedman, M. J. Lab, R. Jones, D. Klenerman and Y. E. Korchev, *Angew. Chem., Int. Ed.*, 2006, **45**, 2212–2216.
73 B. Babakinejad, P. Jönsson, A. López Córdoba, P. Actis, P. Novak, Y. Takahashi, A. Shevchuk, U. Anand, P. Anand, A. Drews, A. Ferrer-Montiel, D. Klenerman and Y. E. Korchev, *Anal. Chem.*, 2013, **85**, 9333–9342.
74 Y. Nashimoto, Y. Takahashi, H. Ida, Y. Matsumae, K. Ino, H. Shiku and T. Matsue, *Anal. Chem.*, 2015, **87**, 2542–2545.
75 D. Momotenko, K. McKelvey, M. Kang, G. N. Meloni and P. R. Unwin, *Anal. Chem.*, 2016, **88**, 2838–2846.
76 D. Perry, D. Momotenko, R. A. Lazenby, M. Kang and P. R. Unwin, *Anal. Chem.*, 2016, **88**, 5523–5530.
77 D. J. Comstock, J. W. Elam, M. J. Pellin and M. C. Hersam, *Anal. Chem.*, 2010, **82**, 1270–1276.
78 Y. Takahashi, A. I. Shevchuk, P. Novak, Y. Murakami, H. Shiku, Y. E. Korchev and T. Matsue, *J. Am. Chem. Soc.*, 2010, **132**, 10118–10126.
79 M. A. O'Connell and A. J. Wain, *Anal. Chem.*, 2014, **86**, 12100–12107.
80 M. Sen, Y. Takahashi, Y. Matsumae, Y. Horiguchi, A. Kumatani, K. Ino, H. Shiku and T. Matsue, *Anal. Chem.*, 2015, **87**, 3484–3489.
81 M. A. O'Connell, J. R. Lewis and A. J. Wain, *Chem. Commun.*, 2015, **51**, 10314–10317.
82 B. P. Nadappuram, K. McKelvey, R. Al Botros, A. W. Colburn and P. R. Unwin, *Anal. Chem.*, 2013, **85**, 8070–8074.
83 Y. Liu, M. Li, F. Zhang, A. Zhu and G. Shi, *Anal. Chem.*, 2015, **87**, 5531–5538.
84 W.-Z. Wu, W.-H. Huang, W. Wang, Z.-L. Wang, J.-K. Cheng, T. Xu, R.-Y. Zhang, Y. Chen and J. Liu, *J. Am. Chem. Soc.*, 2005, **127**, 8914–8915.
85 M. R. Angle and A. T. Schaefer, *PLoS One*, 2012, **7**, e43194.
86 Y.-T. Li, S.-H. Zhang, X.-Y. Wang, X.-W. Zhang, A. I. Oleinick, I. Svir, C. Amatore and W.-H. Huang, *Angew. Chem., Int. Ed.*, 2015, **54**, 9313–9318.
87 Y. T. Li, S. H. Zhang, L. Wang, R. R. Xiao, W. Liu, X. W. Zhang, Z. Zhou, C. Amatore and W. H. Huang, *Angew. Chem., Int. Ed.*, 2014, **53**, 12456–12460.
88 X. Li, S. Majdi, J. Dunevall, H. Fathali and A. G. Ewing, *Angew. Chem., Int. Ed.*, 2015, **54**, 11978–11982.
89 Y. Zhang, J. Clausmeyer, B. Babakinejad, A. López Córdoba, T. Ali, A. Shevchuk, Y. Takahashi, P. Novak, C. Edwards, M. Lab, S. Gopal, C. Chiappini, U. Anand, L. Magnani, R. C. Coombes, J. Gorelik, T. Matsue, W. Schuhmann, D. Klenerman, E. V. Sviderskaya and Y. Korchev, *ACS Nano*, 2016, **10**, 3214–3221.
90 J. Clausmeyer, P. Actis, A. López Córdoba, Y. Korchev and W. Schuhmann, *Electrochem. Commun.*, 2014, **40**, 28–30.
91 Y. Wang, J.-M. Noël, J. Velmurugan, W. Nogala, M. V. Mirkin, C. Lu, M. Guille Collignon, F. Lemaître and C. Amatore, *Proc. Natl. Acad. Sci. U. S. A.*, 2012, **109**, 11534–11539.
92 F. J. M. Hoeben, F. S. Meijer, C. Dekker, S. P. J. Albracht, H. A. Heering and S. G. Lemay, *ACS Nano*, 2008, **2**, 2497–2504.
93 F. J. M. Hoeben, I. Heller, S. P. J. Albracht, C. Dekker, S. G. Lemay and H. A. Heering, *Langmuir*, 2008, **24**, 5925–5931.
94 M. A. G. Zevenbergen, P. S. Singh, E. D. Goluch, B. L. Wolfrum and S. G. Lemay, *Nano Lett.*, 2011, **11**, 2881–2886.
95 S. Kang, A. F. Nieuwenhuis, K. Mathwig, D. Mampallil and S. G. Lemay, *ACS Nano*, 2013, **7**, 10931–10937.
96 K. Mathwig, T. J. Aartsma, G. W. Canters and S. G. Lemay, *Annu. Rev. Anal. Chem.*, 2014, **7**, 383–404.
97 L. Rassaei, K. Mathwig, S. Kang, H. A. Heering and S. G. Lemay, *ACS Nano*, 2014, **8**, 8278–8284.
98 K. Mathwig, Q. Chi, S. G. Lemay and L. Rassaei, *ChemPhysChem*, 2016, **17**, 452–457.
99 J. E. Dick, C. Renault and A. J. Bard, *J. Am. Chem. Soc.*, 2015, **137**, 8376–8379.
100 L. Han, W. Wang, J. Nsabimana, J.-W. Yan, B. Ren and D. Zhan, *Faraday Discuss.*, 2016, DOI: 10.1039/c6fd00061d.
101 S. E. Kleijn, S. C. Lai, M. T. Koper and P. R. Unwin, *Angew. Chem., Int. Ed.*, 2014, **53**, 3558–3586.
102 R. Sardar, A. M. Funston, P. Mulvaney and R. W. Murray, *Langmuir*, 2009, **25**, 13840–13851.
103 K. A. Willets and R. P. Van Duyne, *Annu. Rev. Phys. Chem.*, 2007, **58**, 267–297.
104 W. Cheng and R. G. Compton, *TrAC, Trends Anal. Chem.*, 2014, **58**, 79–89.
105 J. B. Sambur and P. Chen, *Annu. Rev. Phys. Chem.*, 2014, **65**, 395–422.
106 W. Wang and N. Tao, *Anal. Chem.*, 2014, **86**, 2–14.
107 Y. Li, J. T. Cox and B. Zhang, *J. Am. Chem. Soc.*, 2010, **132**, 3047–3054.
108 J. Lakbub, A. Pouliwe, A. Kamasah, C. Yang and P. Sun, *Electroanalysis*, 2011, **23**, 2270–2274.
109 Y. Yu, Y. Gao, K. Hu, P.-Y. Blanchard, J.-M. Noel, T. Nareshkumar, K. L. Phani, G. Friedman, Y. Gogotsi and M. V. Mirkin, *ChemElectroChem*, 2015, **2**, 58–63.
110 P. Sun, F. Li, C. Yang, T. Sun, I. Kady, B. Hunt and J. Zhuang, *J. Phys. Chem. C*, 2013, **117**, 6120–6125.
111 J. Clausmeyer, J. Masa, E. Ventosa, D. Ohl and W. Schuhmann, *Chem. Commun.*, 2016, **52**, 2408–2411.
112 X. Xiao and A. J. Bard, *J. Am. Chem. Soc.*, 2007, **129**, 9610–9612.

113 X. Xiao, F.-R. F. Fan, J. Zhou and A. J. Bard, *J. Am. Chem. Soc.*, 2008, **130**, 16669–16677.
114 J. H. Park, S. N. Thorgaard, B. Zhang and A. J. Bard, *J. Am. Chem. Soc.*, 2013, **135**, 5258–5261.
115 D. Lohse and X. Zhang, *Rev. Mod. Phys.*, 2015, **87**, 981–1035.
116 L. Luo and H. S. White, *Langmuir*, 2013, **29**, 11169–11175.
117 Q. Chen, L. Luo, H. Faraji, S. W. Feldberg and H. S. White, *J. Phys. Chem. Lett.*, 2014, **5**, 3539–3544.
118 Q. Chen, H. S. Wiedenroth, S. R. German and H. S. White, *J. Am. Chem. Soc.*, 2015, **137**, 12064–12069.
119 S. R. German, Q. Chen, M. A. Edwards and H. S. White, *J. Electrochem. Soc.*, 2016, **163**, H3160–H3166.
120 S. R. German, M. A. Edwards, Q. Chen, L. Luo and H. S. White, *Faraday Discuss.*, 2016, DOI: 10.1039/C6FD00099A.
121 Q. Chen, L. Luo and H. S. White, *Langmuir*, 2015, **31**, 4573–4581.
122 W. Nogala, J. Velmurugan and M. V. Mirkin, *Anal. Chem.*, 2012, **84**, 5192–5197.
123 J. Velmurugan, J.-M. Noël, W. Nogala and M. V. Mirkin, *Chem. Sci.*, 2012, **3**, 3307.
124 S. J. Percival and B. Zhang, *Langmuir*, 2014, **30**, 11235–11242.
125 J. Velmurugan, D. Zhan and M. V. Mirkin, *Nat. Chem.*, 2010, **2**, 498–502.